Energy Materials

Supplementary Materials

Tunable crystallinity in cellulose nanofiber-polyethylene oxide electrolyte films for stable quasi-solid-state lithium-metal batteries

Kittima Lolupiman[1], Prasit Pattananuwat[2,3], Manunya Okhawilai[4], Fangjia Zhao[5], Jiaqian Qin[1,2,3,6,*]

[1]International Graduate Program of Nanoscience and Technology (Interdisciplinary), College of Interdisciplinary and Integrative Studies, Chulalongkorn University, Bangkok 10330, Thailand.

[2]Department of Materials Science, Faculty of Science, Chulalongkorn University, Bangkok 10330, Thailand.

[3]Center of Excellence on Advanced Materials for Energy Storage, Chulalongkorn University, Bangkok 10330, Thailand.

[4]Department of Chemical Engineering, Faculty of Engineering, Chulalongkorn University, Bangkok 10330, Thailand.

[5]Department of Chemistry, University College London, London WC1H 0AJ, UK.

[6]Energy Research Institute, Chulalongkorn University, Bangkok 10330, Thailand.

[*]**Correspondence to:** Dr. Jiaqian Qin, Department of Materials Science, Faculty of Science, Chulalongkorn University, Bangkok 10330, Thailand. E-mail: jiaqian.q@chula.ac.th

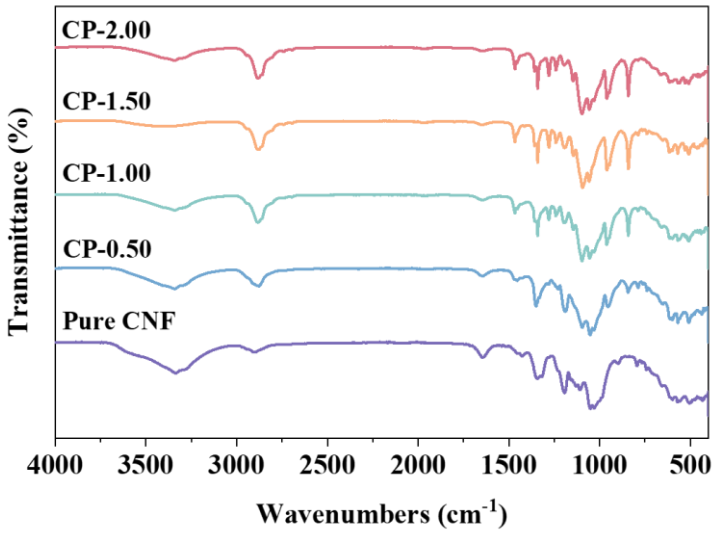
ORCID: Jiaqian Qin (0000-0002-9166-3533)

The preparation of quasi-solid polymer electrolyte (SPE) films was using a 2.5 wt.% cellulose nanofiber (CNF) solution 20 g combined with varying amounts of polyethylene oxide (PEO), as shown in Supplementary Table 1, to obtain the samples designated as Pure CNF, CP-0.50, CP-1.00, CP-1.50, and CP-2.00, respectively.

Supplementary Table 1. Mass ratio of CNF solution: PEO and CNF: PEO

Sample	Mass ratio of	Mass ratio of
	CNF solution (g): PEO (g)	CNF (g): PEO (g)
Pure CNF	20:0	0.5:0
CP-0.50	20:0.5	0.5:0.5
CP-1.00	20:1.0	0.5:1.0
CP-1.50	20:1.5	0.5:1.5
CP-2.00	20:2.0	0.5:2.0

The full-range FT-IR spectra of the CNF/PEO quasi-SPE films. The spectra confirm characteristic functional groups from CNF, PEO, and LiTFSI-based electrolyte components, indicating successful formation of the Quasi-SPE films.



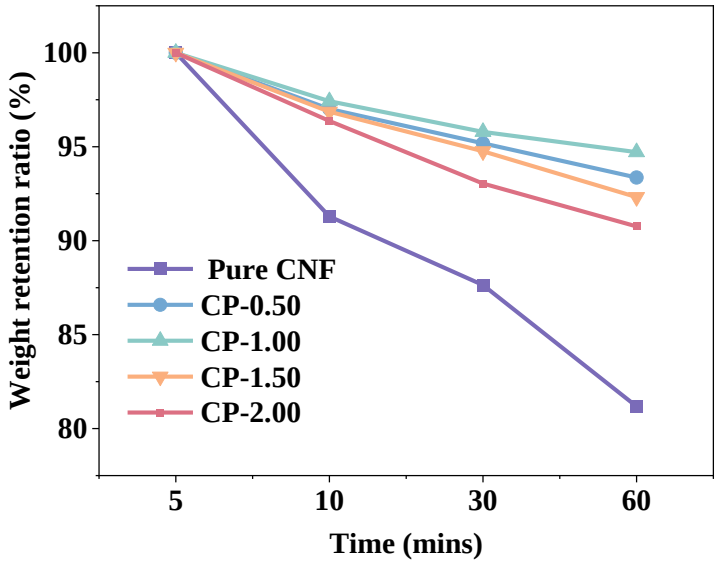
Supplementary Figure 1. FT-IR spectra of the quasi-solid electrolyte films in the range of 4000-500 cm^{-1}.

Supplementary Table 2. Electrolyte uptake of quasi-SPE films

Quasi-SPE electrolyte films	Weight dry (W_{dry})	Weight wet (W_{wet}) After drying 5 mins	Electrolyte uptake (%)
Pure CNF	23.2	35.6	53.44
CP-0.50	31.8	60.2	89.3
CP-1.00	38.4	73.7	91.92
CP-1.50	47.1	85.9	82.37
CP-2.00	54.9	96.3	75.4

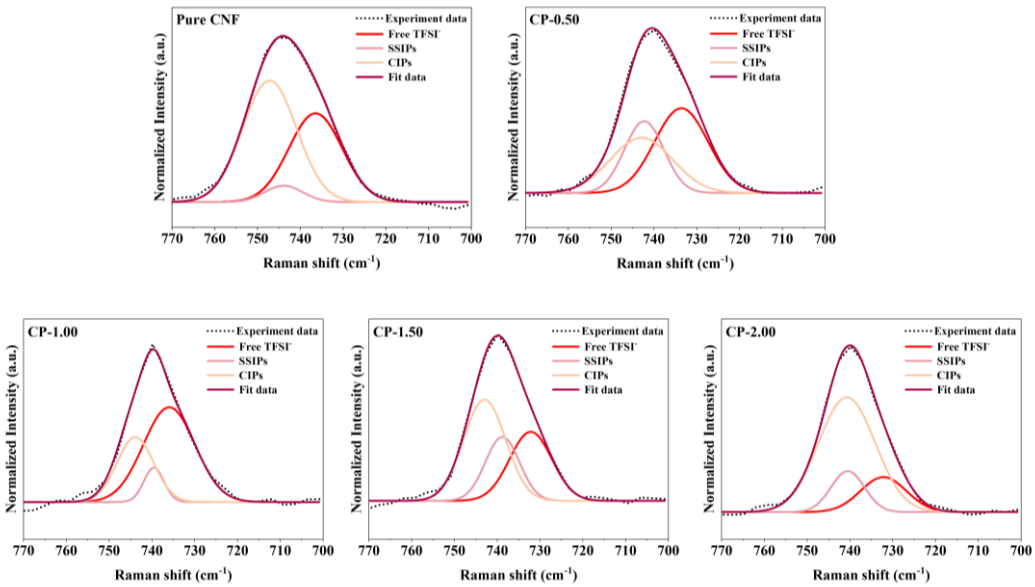
The electrolyte uptake of the Quasi-SPE electrolyte films exhibited a non-monotonic trend, initially increasing with the addition of CP and subsequently declining beyond optimal loading. The uptake rose from 53.44% for pure CNF to a maximum of 91.92% for CP-1.00. This enhancement is attributed to the synergistic interaction between the CNF framework and PEO chains, which reduces the overall crystallinity, increases the amorphous phase, and constructs a well-connected 3D network that facilitates electrolyte penetration. However, further increasing the CP content led to a decrease in electrolyte uptake to 82.37% for CP-1.50 and 75.4% for CP-2.00. This reduction is driven by a pore-blocking effect and excessive polymer chain aggregation, which creates a denser film matrix and diminishes the accessible free volume for liquid electrolyte absorption. Consequently, CP-1.00 represents the optimal composition, offering the highest electrolyte retention capacity.

We evaluated the electrolyte retention stability of quasi-SPE films over a drying period of 5-60 min at 40 ºC. Pure CNF showed significant weight loss, with the retention ratio dropping to ~81.18% after 60 min due to rapid solvent evaporation. In contrast, all quasi-SPE films showed impressive retention performance (>90.76% after 60 mins), with CP-1.00 maintaining the highest retention ratio (94.71%), confirming that polymer incorporation, with a balance of crystalline and amorphous regions, effectively mitigates electrolyte evaporation and enhances structural solvent confinement.



Supplementary Figure 2. Electrolyte retention stability of quasi-SPE films.

To examine the interaction between Li^+ and $TFSI^-$, various $TFSI^-$ ion pairs were defined by bending vibration positions. The peaks located at 733 to 738 cm^{-1}, 738 to 742 cm^{-1}, and 743 to 746 cm^{-1} could be attributed to free TFSI–, SSIPs, and CIPs, respectively. CP-1.00 represents the optimal PEO content, which has the highest free ions and thus affects the ionic conductivity and battery performance.



Supplementary Figure 3. Zoom-in Raman spectra in the range of 770-700 cm^{-1}.

Supplementary Table 3 summarizes the bulk resistance (R_β), electrode contact area (A), film thickness (L), and ionic conductivity (σ) of the quasi-SPE films. The Pure CNF film had a thickness of 0.005 cm, whereas all CNF/PEO films had a thickness of 0.02 cm. Pure CNF exhibited the lowest ionic conductivity of 10^{-6} S·cm^{-1}, which was attributed to the highly crystalline cellulose structure that restricted Li^+ migration. After incorporation of PEO, the ionic conductivity significantly increased and reached a high value of 10^{-4} S·cm^{-1}.

Supplementary Table 3. The parameters (R_β, A, L, and σ) of the quasi-SPE film

Pure CNF		**CP-0.50**		**CP-1.00**		**CP-1.50**		**CP-2.00**	
R_b	5.37E+02	R_b	1.56E+01	R_b	6.56E+01	R_b	1.90E+01	R_b	2.92E+02
A	1.54E+00	A	1.54E+00	A	1.54E+00	A	1.54E+00	A	1.54E+00
L	5.00E-03	L	2.00E-02	L	2.00E-02	L	2.00E-02	L	2.00E-02
σ	6.05E-06	σ	8.33E-04	σ	1.98E-04	σ	6.84E-04	σ	4.45E-05

Supplementary Table 4. Ionic conductivity values of the quasi-SPE films at different temperatures

Sample	**Temperature**		
	25 ºC	**40 ºC**	**60 ºC**
Pure CNF	2.34E-06	7.12E-06	3.00E-05
CP-0.50	4.36E-04	8.78E-04	2.45E-03
CP-1.00	2.12E-04	3.55E-04	1.31E-03
CP-1.50	3.32E-04	5.30E-04	1.83E-03
CP-2.00	4.27E-05	6.65E-05	3.38E-04

The ionic conductivity of quasi-SPE films was evaluated at 25, 40, and 60 °C. The increase in conductivity with temperature. These conductivity data were further analyzed using the Arrhenius equation to calculate the activation energy.

The Arrhenius parameters obtained from the temperature-dependent ionic conductivity measurements are summarized. The slope values were obtained from the linear fitting of the Arrhenius plots (ln σ versus 1000/T), and the corresponding activation energies were calculated using the Arrhenius equation. The high correlation coefficients (R^2) indicate good agreement between the experimental conductivity data and the fitted model. The activation energy values represent the energy barrier required for ionic migration within the electrolyte matrix.

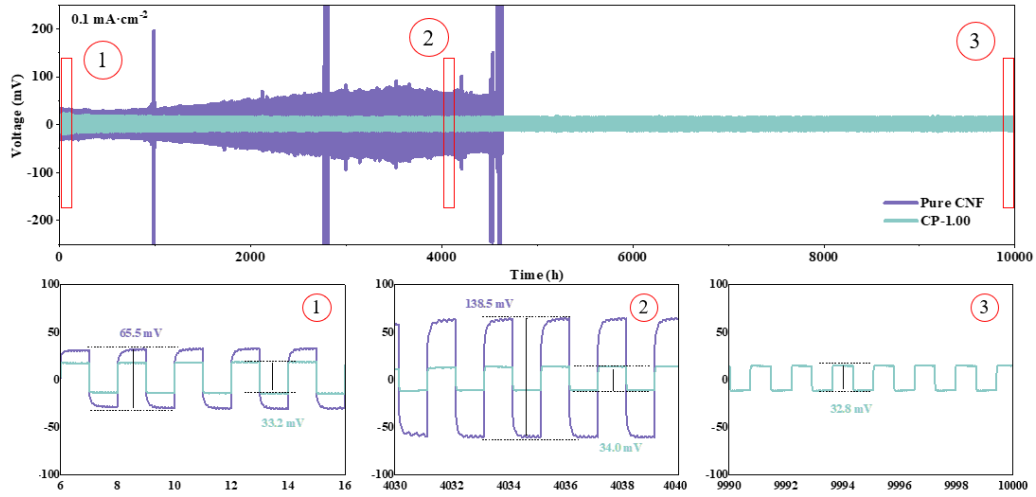
The activation energy (E_a) was determined from the Arrhenius plots obtained by plotting ln(σ) as a function of 1000/T. The linear fitting slope was used according to the modified Arrhenius equation and the activation energy was calculated using Equation (1).

$$E_a = -(slope) \times 1000 k_B \qquad (1)$$

where k_B is the Boltzmann constant (8.617×10^{-5} eV·K^{-1}). The fitting slopes, correlation coefficients (R^2), and activation energy are summarized in Supplementary Table 5.

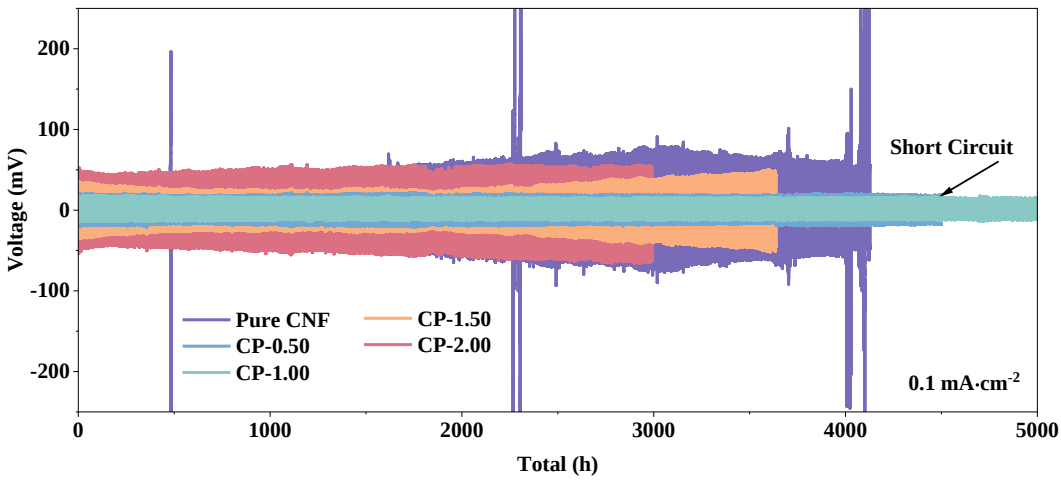
Supplementary Table 5. Arrhenius fitting parameters and activation energy obtained from ionic conductivity measurements

Sample	Slope	R^2	Activation energy (eV)
Pure CNF	-7.25	0.99	0.62
CP-0.50	-4.92	0.99	0.42
CP-1.00	-5.23	0.96	0.45
CP-1.50	-4.9	0.95	0.42
CP-2.00	-5.95	0.92	0.51



Supplementary Figure 4. Galvanostatic lithium stripping and plating for Li|| pure CNF ||Li and Li|| CP-1.00 ||Li Zoom-in regions 1, 2, and 3.

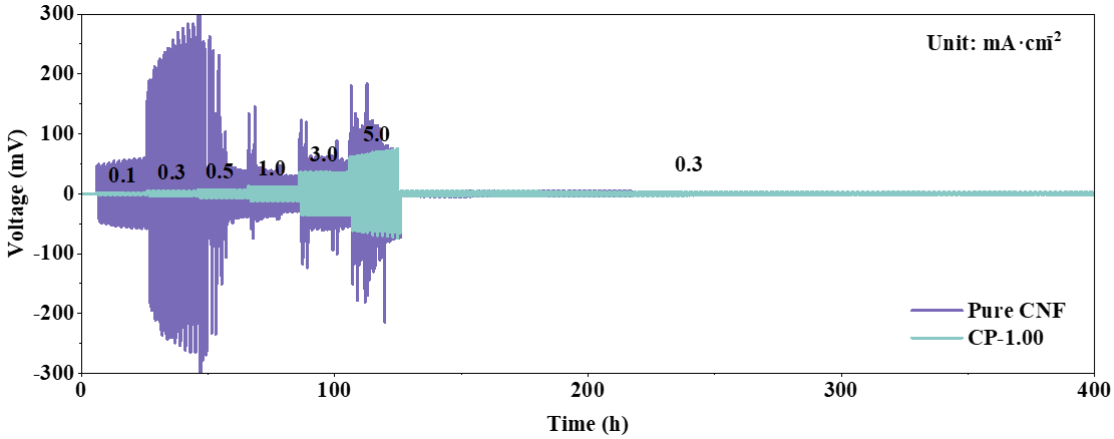
The pure CNF cell exhibits large overpotential and sharp spikes, indicating unstable Li plating/stripping, increasing interfacial resistance, and possible dendrite/void formation. In contrast, the CP samples exhibit much smoother, lower-voltage polarization, especially CP-1.00, which maintains the most stable voltage profile over long cycling up to 5000 h.



Supplementary Figure 5. Galvanostatic lithium stripping and plating measurement at 0.1 mA·cm^{-2} of quasi-solid electrolyte.

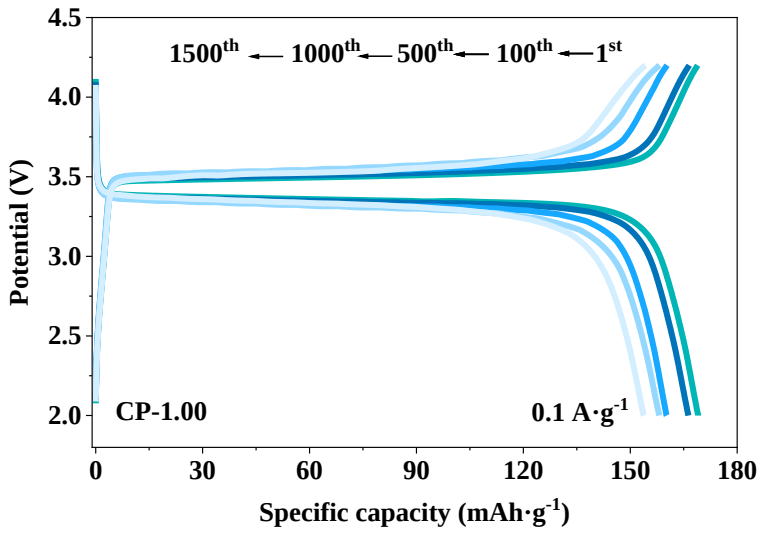
To investigate the cyclic stability of quasi-solid electrolytes with a Li-metal anode, Li|| pure CNF ||Li and Li|| CP-1.00 ||Li symmetric cells were assembled for plating and

stripping tests to measure the stability with increasing steps of current density from 0.1 $mA \cdot cm^{-2}$ to 5 $mA \cdot cm^{-2}$. The charge and discharge time is 1 hour. The CP-1.00 showed greater stability than pure CNF.



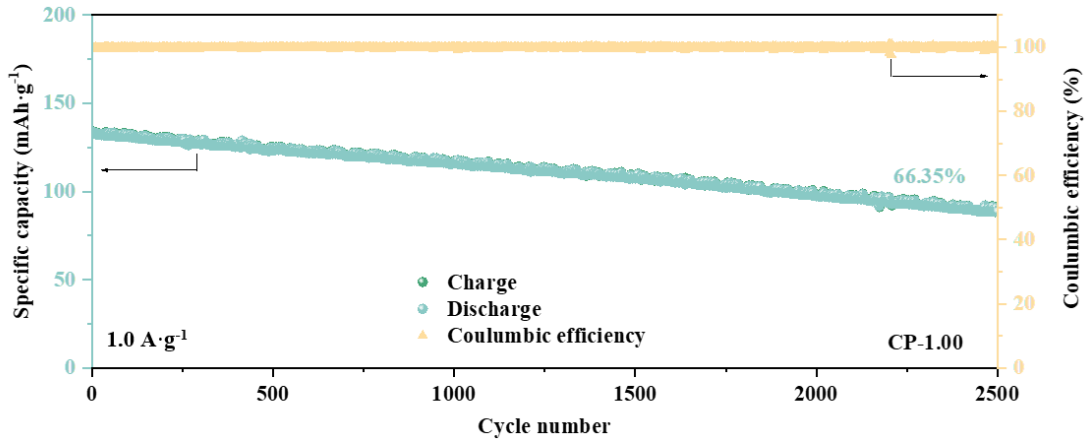
Supplementary Figure 6. Cycling stability of Li||Li symmetric cells.

The long-term galvanostatic charge–discharge profiles of the Li||CP-1.00||LFP cell from the 1st to 1500th cycle are presented in Supplementary Figure 7. The curves retain their characteristic flat plateaus with negligible capacity decay and minimal voltage gap expansion over extended cycling. This stable behavior demonstrates that the CP-1.00 successfully suppresses side reactions and maintains structural integrity. Consequently, it delivers excellent electrochemical durability throughout the 1500th cycle test.



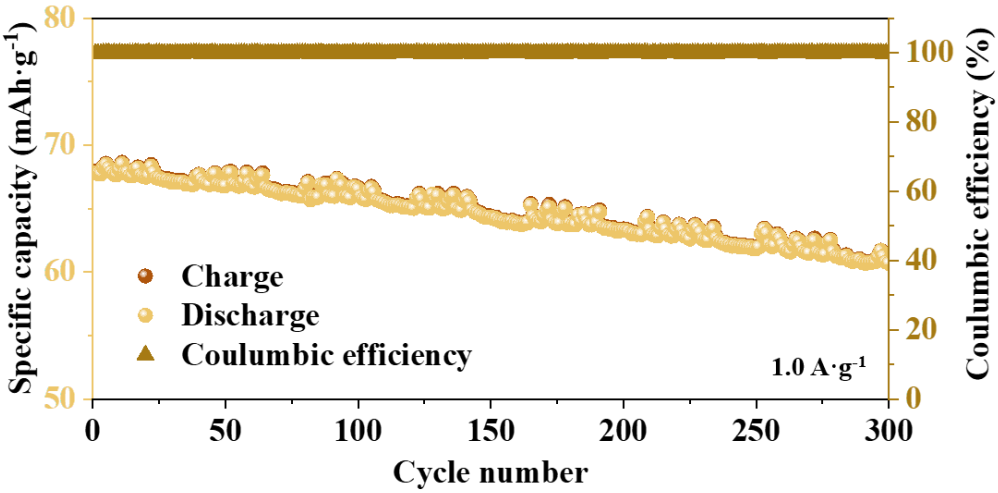
Supplementary Figure 7 Galvanostatic Charge and discharge voltage profiles of Li|| CP-1.00 ||LFP at 1st, 100th, 500th, 1000th, and 1500th, respectively.

CP-1.00 shows impressive long-term cycling stability at a high current density of 1.0 $A \cdot g^{-1}$, delivering a discharge capacity of 133.76 $mAh \cdot g^{-1}$ and retaining 66.35% capacity over 2,500 cycles. This outstanding cycling performance shows the optimized CNF/PEO electrolyte framework can maintain stable Li^+ transport pathways and a robust electrode–electrolyte interface under high-rate cycling conditions. The improved stability is attributed to the balanced crystalline and amorphous structure of CP-1.00, which facilitates ion migration while preserving structural integrity during prolonged operation.

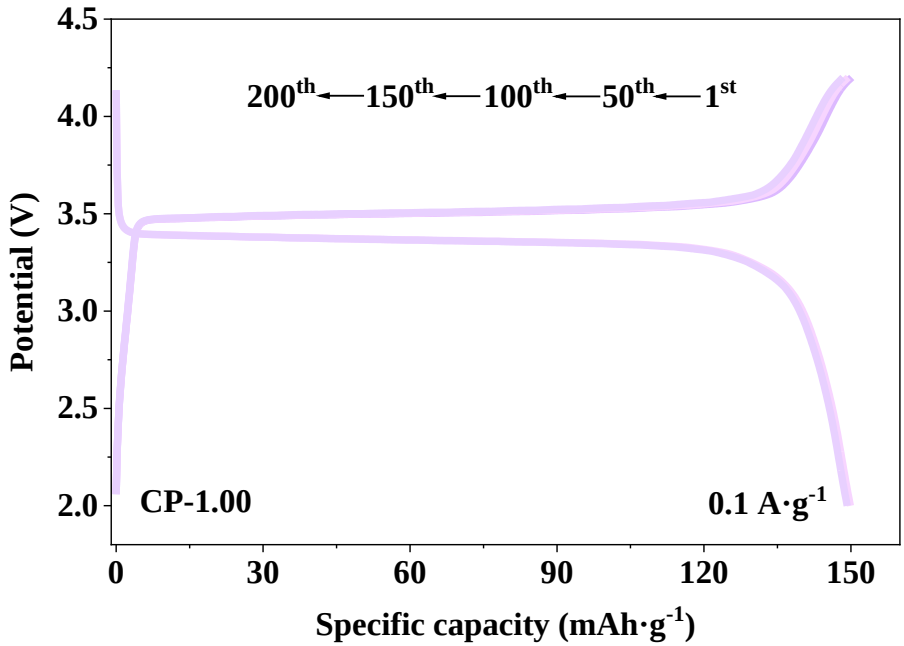


Supplementary Figure 8. Long-term cycling of Li|| CP-1.00 ||LFP.

To evaluate the commercial separator under lean electrolyte conditions, we assembled a control cell with Celgard 2325 as the separator and a restricted liquid electrolyte volume of 10 μL (matching the volume used in the quasi-SPE system). The cell delivers a lower initial discharge capacity of ~68 $mAh \cdot g^{-1}$ at 1.0 $A \cdot g^{-1}$ and shows continuous capacity decay to ~60 $mAh \cdot g^{-1}$ over 300 cycles, with noticeable fluctuations in cycling stability. This inferior performance is attributed to poor electrolyte volume and incomplete wetting of the commercial separator, leading to uneven ion transport.

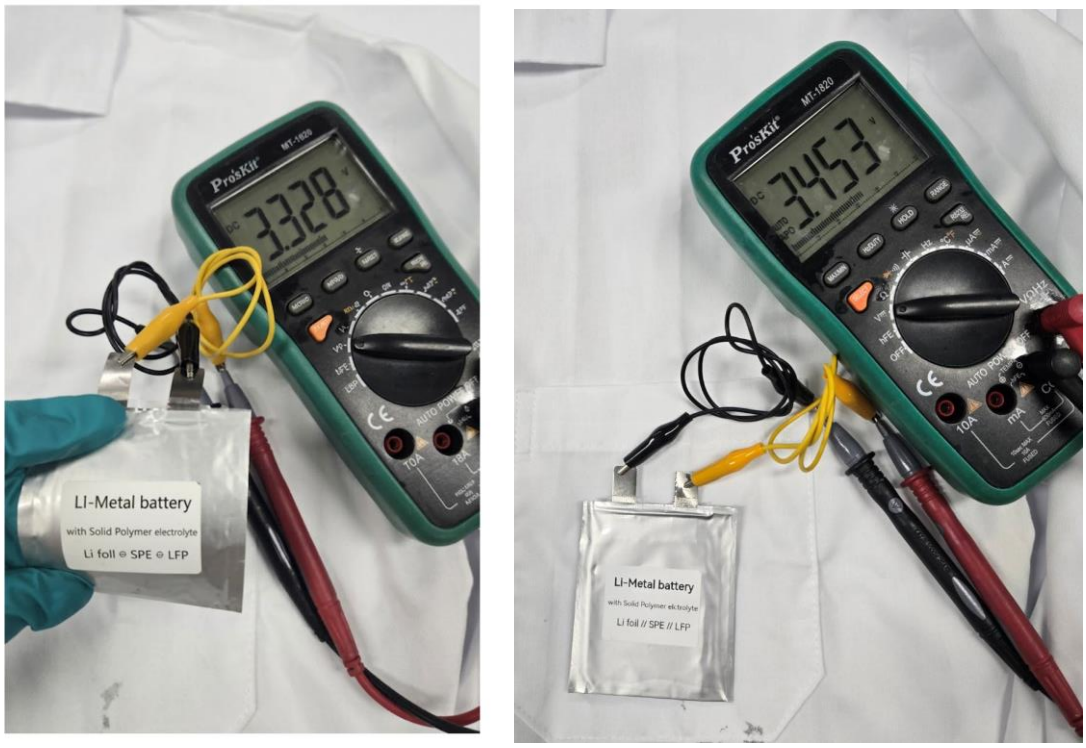


Supplementary Figure 9. Long-term cycling of Li|| Celgard2325 ||LFP.



Supplementary Figure 10. Galvanostatic Charge and discharge voltage profiles of Li|| CP-1.00 ||LFP pouch cell battery at the 1st, 50th, 100th, 150th, and 200th cycles, respectively.

The exact initial open-circuit voltage (OCV) of the assembled pouch cell was measured to be in the range of 3.32–3.45 V. We have updated the corresponding sentence in the manuscript to replace "around 3.3xx V" with the range 3.32–3.45 V.



Supplementary Figure 11. Digital photographs of the pouch cell battery with an initial open-circuit voltage (OCV) of 3.32- 3.45 V, taken by the authors.